Recent advances in performance and effect of Zr doping with ZnO thin film sensor in ammonia vapour sensing

Jafar Ali Ibrahim S.[1,*], Rajasekar S.[2,*], Varsha[3,*], Karunakaran M.[4], Kasirajan K.[4], Kalyan Chakravarthy N.S.[1], Kumar V.[5,*] and Kaur K.J.[6]

[1]QIS College of Engineering and Technology, Vengamukkapalem, Ongole - 523 272, India

[2]QIS Degree and PG College, Vengamukkapalem, Ongole - 523 272, India

[3]Department of Computer Science Engineering, CT Institute of Engineering, Management and Technology, Jalandhar, Punjab, India

[4]PG &Research Department of Physics, Alagappa Govt Arts College, Karaikudi - 630 003, India

[5]Department of Applied Sciences, CT Institute of Engineering, Management and Technology, Shahpur Campus Jalandhar, Punjab, India
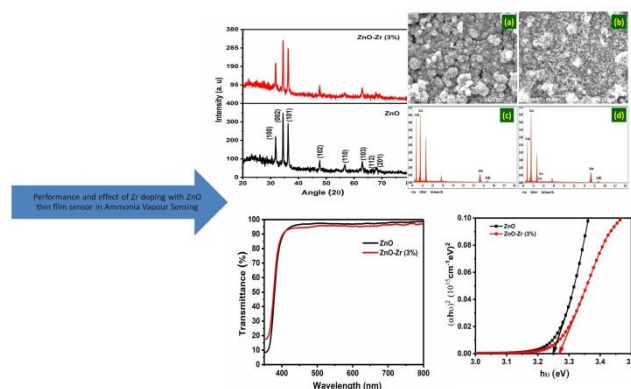
[6]Department of Chemistry, Sri Guru Gobind Singh College, Sector 26, Chandigarh 160019, India

Received: 28/09/2021, Accepted: 30/10/2021, Available online: 09/11/2021

*to whom all correspondence should be addressed: e-mail: jafartheni@gmail.com; rajasekarsaec@gmail.com; varsha.548@ctgroup.in; vaneet2106@gmail.com

https://doi.org/10.30955/gnj.004020

Graphical abstract

Abstract

Pure and Zr doped ZnO thin films were prepared using SILAR technique. The influence of Zr doping on structural, morphological, optical and gas sensing properties of ZnO has been reported in this study. X-ray diffraction study confirmed the formation of wurtzite structure of ZnO thin film (JCPDS 36-1451) fabricated by SILAR (Successive Ionic Layer by Adsorption and Reaction) technique and the caluculated crystallites size of pure and doped ZnO were 39 and 36 nm respectively. SEM analysis of thin films has shown a completely different surface morphology. EDAX spetrum cnfirmed the presence of different compositional element in the fabriated thin films. Zr (3 wt%) doped ZnO thin film exhibited the best properties with a good transmittance and it has wide band gap of 3.26 eV. Photoluminescence emissions indicated increase in concentration of oxygen vacancies with introduction of dopant. NH_3 vapour sensors were fabricated out of fabricated samples and it was observed that doped samples have significantly high sensing response, good selectivity, fast response and recovery time to ammonia vapoutr at room temperature.

Keywords: Zr, ZnO, SEM, NH3, EDAX , SILAR.

1. Introduction

The ammonia gas exposure with high sensitivity have been highly demanded nowadays, since ammonia is a commonly utilized toxic gas in various industrial sectors such as plastics, fertilizers, explosives, textiles, pesticides, food-based, and refrigerant systems and highly toxic and corrosive agent. These agents can threat human health and environment (Gong *et al.*, 2019; Jayababu *et al.*, 2018; Kwak *et al.*, 2019; Mani and Rayappan, 2015). The metal oxide semiconductors such as SnO_2, ZnO, TiO_2, WO_3, Bi_2O_3, etc based solid state gas sensors are extensively used and it is currently constituting one of the most investigating groups of materials in gas detecting device (Wang *et al.*, 2010). Semiconductor metal oxides based gas sensors have been widely investigated due to their small size, low cost and compatibility with semiconductor fabrication technology. Gas sensors are working on the simple basic principle i.e. the electrical conductivity of a semiconducting metal oxide varies with the composition and the concentration of the gas atmosphere, surrounding it. Amongst various semiconducting metal oxides, ZnO has been extensively studied for the detection of various gases, such as H_2, CO, NH_3, NO_2, and ethanol vapors due to its high mobility of conduction electrons and good chemical and thermal stability under the operating conditions (Hyojin *et al.*, 2010).

ZnO has several applications, such as related to surface acoustic wave devices, piezoelectric devices, varistors, planar optical waveguides, transparent electrodes, UV photo detectors, facial powders, gas sensors, etc. It is an n-type semiconductor of wurtizite structure with direct band gap of about 3.37eV and (Hyojin et al., 2010). It has been

demonstrated that the electrical and sensing characteristics of ZnO films can be controlled by doping with various elements or by heat treatment processes (Dighavkar, 2013; Lukas and Judith, 2007; Karmakar et al., 2007; Norris et al., 2003; Wang et al., 2006; Chao et al., 2019; Singh et al., 2020; Paraguay *et al.*, 2000; Bahsi and Oral, 2007; Al-Hardan *et al.*, 2009; Corlu *et al.*, 2017; Sankar Ganesh *et al.*, 2017; Zhao *et al.*, 2011). The ionic radius of Zr^{+4} (0.8 Å) is larger than Zn^{+2} (0.74 Å). Doping ZnO films with Zr decreases carrier concentration and improves transparency in the visible range (Bharath et al., 2018; Lee *et al.*, 2006). ZnO-based thin films have been prepared by various thin film deposition techniques, such as RF/DC magnetic sputtering deposition, pulsed laser deposition, chemical vapor deposition, chemical bath deposition, SILAR, spray pyrolysis, sol-gel methods, etc. SILAR technique is the most useful method to prepare ZnO thin films. It has the superior advantages such as economical, relatively very simple, high purity reproducibility, does not require high-quality substrates and high-cost equipment than the other methods (Qadri et al., 2000). In this work, polycrystalline semiconductor thin films of pure and Zr-doped ZnO were prepared by SILAR method and the effects of Zr doping on crystallinity, microstructure, surface morphology, optical transparency, photoluminescence were studied and the effect of Zr doping on ZnO and its sensor performance were reported.

2. Experimental

2.1. Preparation of thin film

In this work, pure and 3% Zr-doped ZnO thin films were prepared by Successive Ionic Layer by Adsorption and Reaction method on glass substrates. 3 wt% of Zr sample exhibits the best response and recovery time of 28 and 8 s. Highly pure zinc sulphate (ZnSO4, 99.3 Pure Regeant Grade, Loudwolf) and sodium hydroxide (NaOH, 99.99 % Pure, Merk Pvt Ltd.) were used as a host zinc precursor and oxidizing agents, respectively. Zinc sulphate with 0.1 M concentration was dissolved in deionized water (50 mL) and stirred for 10 min at room temperature to obtain saturated and clear transparent solution with pH 9 ± 0.2 and NaOH with 0.2 M concentration and equal amount was added to the prepared solution. This forms the sodium zincate bath and the pH value of the sodium zincate solution is 9±0.2. Normal SILAR system consists of four beakers, but modified SILAR system has only two beakers (Radhi Devi *et al.*, 2020). The first beaker includes precursor solution, and second beaker has hot water. Firstly, a well cleaned glass substrate was vertically immersed into the sodium zincate bath for 20 s. In the second step the substrate was dipped into the double-distilled hot water maintained at 900C for 10 s to remove the loosely adsorbed ions. The cycles depicted above were performed for a known number of times (80 dipping cycles) to obtain the desired film thickness. In this method we found the pure ZnO thin films. Furthermore, the same procedure was applied to prepare zirconium-doped zinc oxide thin with different doping concentration 3%. The dopant precursor

zirconium (IV) oxychloride octahydrate $(Cl_2H_{18}O_9Zr)$ was added to a sodium zincate (zinc sulphate + NaOH) solution.

3. Results and discussions

3.1. X-Ray diffraction studies

The crystalline nature of and structure of pure and Zr doped ZnO thin films were identified by X-ray diffraction studies using Bruker (D8 Advance Eco XRD) with Cu Kα radiation (λ=1.54056Å). Figure 1 shows the X-Ray diffraction patterns of pure and Zr-doped ZnO thin films. It reveals that ZnO exhibits a hexagonal wurzite structure and is confirmed by the diffraction peaks at (100), (002) and (101) planes and well fit with JCPDS 36-1451. It is observed that the intensities of diffraction peaks decrease with Zr doping. The crystallite size of all the deposited films is calculated by using the very well known Scherrer's formula (Sankar Ganesh *et al.*, 2018).

$$D = \frac{0.9\lambda}{\beta \cos\theta} \tag{1}$$

Where, D is the crystallite size, λ is the wavelength of the X-ray used (CuKα =1.54056 Å), β is the full with at half maximum intensity and θ is the peak position.

The defects like strain (ε) and dislocation density (δ) for the ZnO:Zr was evaluated using the relations

$$\varepsilon = \frac{\beta \cot\theta}{4} \tag{2}$$

$$\delta = \frac{1}{D^2} \tag{3}$$

And the number of crystallites (n_c) as

$$n_c = \frac{t}{D^3} \tag{4}$$

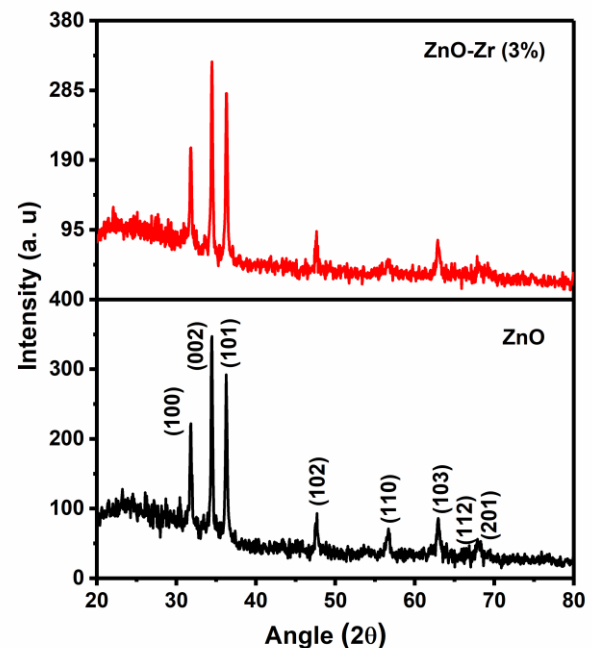where, t is the film thickness.

Figure 1. X-Ray diffraction pattern of pure and Zr doped ZnO thin film.

The unit cell volume '*V*' and lattice constants '*a*' and '*c*' of the hexagonal phase of ZnO and Zr doped ZnO films was determined by the following relations (Hong *et al.*, 2019).

$$V = a^2 c \, (\sin 60°) \tag{5}$$

$$\frac{1}{d^2} = \frac{4}{3} \left\{ \frac{h^2 + hk + k^2}{a^2} \right\} + \left\{ \frac{l^2}{c^2} \right\} \tag{6}$$

Where, *(hkl)* and *d* have their usual meanings.

The calculated microstructural parameters of pure and Zr doped ZnO thin films were summarized in Table 1. The average crystallite size was found to be 39 and 36 nm pure and 3 at% Zr doped thin film respectively and noted that Zr-doped ZnO thin films have reduced average crystallite size. It was also noted that the (001) and (002) peaks slightly shifted towards the lower diffraction angle after Zr doping. It has been observed that Zr doping can increase the 'a' and 'c' lattice parameters of ZnO films. The 'a' and 'c' lattice parameters are 3.005 Å and 5.204 Å for pure ZnO films and increase gradually to 3.006 Å and 5.206 Å for 3 at% Zr

doped ZnO thin films. Zr doping can increase the lattice parameters of unit cells due to the ionic radius of Zr^{+4} (0.8 Å) is larger than that Zn^{2+} (0.74 Å) (Sankar Ganesh *et al.*, 2018).

3.2. Morphological analysis

The surface morphologies were investigated by (EVO18 CARL ZEISS) Scanning electron microscope (SEM) the image of pure and Zr doped ZnO thin film shown in Figure 2(a-b). The surface morphology of pure ZnO film posses particles of different sizes with pinhole nature all over the surface of the film and due to doping of 3 wt% Zr, the surface appears with a combination of small and medium-size grains and fibre like structure. The pictures also reveal that Zr doping in ZnO films can markedly reduce the average grain size; this finding agrees with XRD measurements. The SEM images clearly revealed that the influence of the Zr doping in ZnO thin films. EDAX analysis of pure and Zr doped ZnO thin film shown in Figure 3(c-d) confirm the presence of element in the prepared films and Zn, O, and Zr peaks were confirming the existence of Zinc (Zn), Oxygen (O) and (Zr) Zirconium in the prepared thin film. The appearance of un-identified Si and Ca peaks at 1.8 KeV and 3.8 KeV owing to the glass substrate.

Table 1. Microstructurl Parameters of pure and Zr doped ZnO thin film

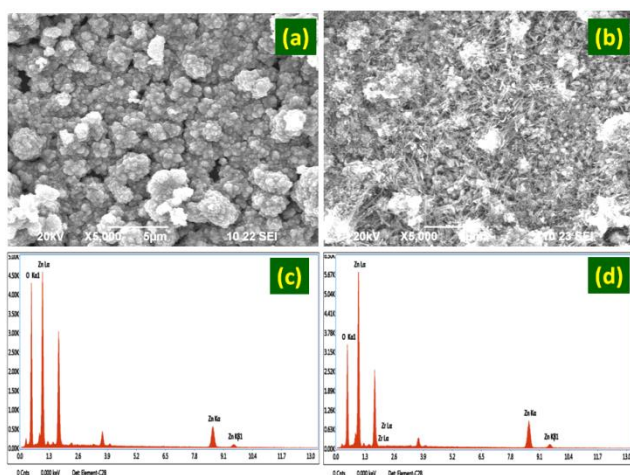| Micro Structural Parameters		ZnO	ZnO-Zr (3 wt. %)
Film Thickness (*nm*)		920	860
Crystallite size (*nm*)		39	36
Dislocation density (×10^{15}) lines.m^{-2}		0.6527	0.7706
Strain (×10^{-3})		2.99	3.25
Number of crystallites (×10^{16}m^{-2})		1.5343	1.8398
Lattice constants(*Å*)	a	3.00507	3.00621
	c	5.20493	5.20691
Cell volume (*Å*)^3		40.7055	40.7520
Band gap (*eV*)		3.24	3.26

Figure 2. SEM and EDAX Analysis of pure and Zr doped ZnO thin film.

3.3. UV–Vis transmittance analysis

The optical transmittance spectra of the pure and Zr doped ZO films, with wavelengths from 200 to 800 nm was recorded by using Ocean Optics HR 2000 and shown in

Figure 3. It indicated that both pure and Zr-doped films exhibited better transparency. It is observed that Zr doping change the transparency of the fabricated thin film and it reveals that the surface morphology has a strong influence on the transparency properties of ZnO films (Vijayprasath *et al.*, 2014). Figure 4 shows the Tauc plot of pure and Zr doped ZnO thin films and the band gap values were extrapolated from the straight sections of the plot of $(\alpha h\upsilon)^2$ersus photo energy $h\upsilon$ (Vijayprasath *et al.*, 2014). It shows that band gap increases slightly from 3.24 to 3.26 eV for ZnO films doped with Zr and it is due to the effect of average crystallite sizes.

3.4. Photoluminescence analysis

Photoluminescence (PL) spectrum was recorded using Varian Carry Eclipse Photo Luminescence spectrophotometer and observed with 380 nm excitation wavelength. Figure 4 shows photoluminescence spectra of pure and Zr doped ZnO thin film. The emission spectrum consists of sharp peaks at 414, 488, 505, and 529 nm and three small peaks at 440, 447, and 541 nm. The peak intensities decrease with the doping percentage. Different types of intrinsic defects are possible in the ZnO structure

which worthy of studying for gas sensing applications (Lee and Park, 2003; Tauc *et al.*, 1966). The peaks 414 nm, 488 and 482 nm are attributed to near band edge (NBE) emission in the UV region due to the recombination of free excitons and emissions related to zinc interstitial respectively. The peak around 541 nm corresponds to oxygen vacancies (Vo). Further, peak at 447 nm and 505 nm belong to zinc interstitials, oxygen vacancies (Vo) (Nkosi *et al.*, 2020; Patil *et al.*, 2019). Thus Zr doping will create the various defect centers in ZnO thin films that will facilitate the sensing of vapor due to their number of active sites (Figure 5).
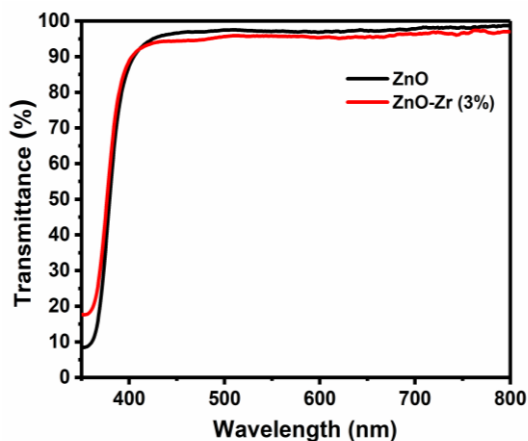

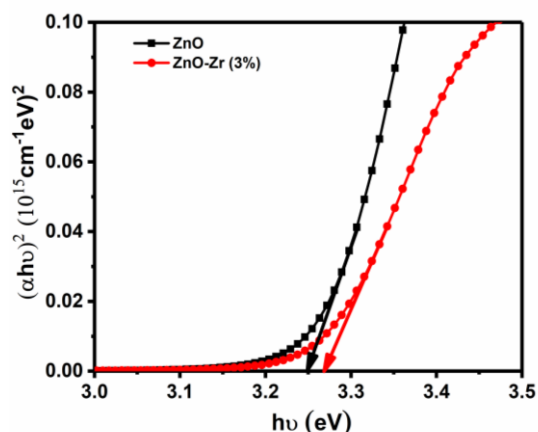**Figure 3.** UV Transmittance spectra pure and Zr doped ZnO thin film.

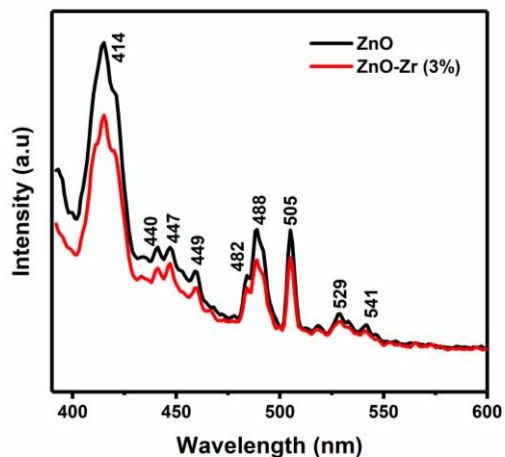**Figure 4.** Band gap of pure and Zr doped ZnO thin film.

Figure 5. PL spectra of pure and Zr doped ZnO thin film.

Photoluminescence emissions are very important for intrinsic and extrinsic transitions in different type of optical characterization techniques because of its non-destructive nature and ability to yield valuable information (Naushad, 2014; Naushad *et al.*, 2015; Naushad *et al.*, 2015; Naushad *et al.*, 2019; Naushad and ALOthman, *2015*).

3.5. NH₃ vapour sensing studies

The home-made setup and a high resistance electrometer (Keithley- 2450) are used to study NH$_3$ vapor sensing properties of pure and Zr doped ZnO thin films (Anita *et al.*, 2016) and Figure 6 shows the schematic representation of sensor setup used in this study. In the sensing chamber, vapor-producing tube and silver pasted fabricated pure and Zr doped thin film sensor are placed. The electrical contacts made by silver pasted end in the fabricated thin film are connected to the computerized high resistance electrometer (Keithley electrometer 2450, USA). Initially the air resistance was measured in the chamber in the open condition and, the required concentration (ppm) of NH$_3$ was inserted using the chromatographic syringe. The NH$_3$ vapor was produced from the tube and is allowed to pass through the fabricated tin film sensor in the chamber. The variation in the resistance was continually recorded with ppm concentration of vapor was introduced into the chamber and also the shift in resistance was calculated after sensing chamber was evacuated. Figure 7 Shows the response and recovery time of deposited pure and Zr doped ZnO thin film on Ammonia vapor sensing at different ppm with time. In this study, pure and Zr doped ZnO thin films were estimated to react to 100 ppm of ammonia by documenting the change in resistance concerning baseline resistance. The vapour sensor system adsorbs or desorbs surface oxygen from pure and Zr doped ZnO thin films and interchanges charge between adsorbed gas, and the thin film layer. This interchange mechanism contributes to changes in the depletion layer and changes in surface or grain boundary. In the experiment, the main reasons for the change in the vapour sensor's electrical properties appear to be the oxygen contribution (Renitta and Vijayalakshmi, 2017; Devi *et al.*, 2020; Krishnan *et al.*, 2017; Shingange *et al.*, 2016; Mani and Rayappan, 2014). In Zr (3 wt. %)-doped ZnO film, the responsivity for NH$_3$ vapor sensing is more due to the reduction in the contact resistance. Hence, more electrons are injected when ammonia reacts with oxygen species. Therefore, the resistance (Rg) decreased is more compared to the undoped ZnO film. Thus, Zr-doped ZnO films are more sensitive to NH$_3$ vapor than pure ZnO film. Table 2 shows the NH$_3$ vapor sensing properties of fabricated thin films. The response time is improved from 59 to 46 seconds and also recovery time reduced from 13 to 6 seconds. Based on the abovementioned reactions, it can be seen clearly that an Zr doping on ZnO can provide more efficient gas adsorption sites and sensitivity improved from 1210 to 1870%. Low-cost and effective materials search for NH3 vapor sensing is very essential for harmful gases monitoring. NH$_3$ is one of the most important chemicals for this purpose. However according to Occupational Safety and Health Administration exposure limit of ammonia to

humans is 35 ppm for 10 min, beyond this limit NH3 is harmful for our environment (Pandey, 2016; Pandey *et al.*, 2015; Pandey *et al.*, 2016).
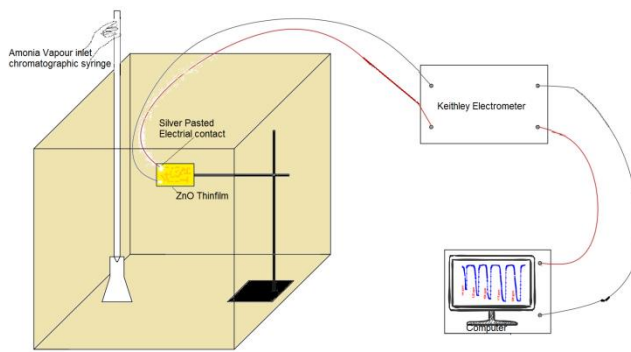

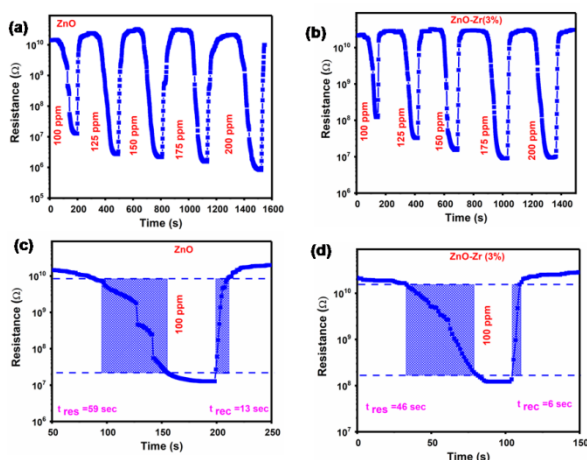**Figure 6.** Schematic of Ammonia vapour sensing setup.

Figure 7. Response and recovery time of deposited pure and Zr doped ZnO thin film on Ammonia vapour sensing.

Table 2. Ammonia vapour sensing properties

NH$_3$ Sensing Properties	ZnO	ZnO-Zr (3%)
Response Time *(Sec)*	59	46
Recovery Time *(Sec)*	13	6
Sensitivity *(%)*	1210	1870

4. Conclusions

The pure and Zr doped ZnO thin films have been successfully synthesized using the SILAR technique. Both pure and Zr doped ZnO thin films were crystallized with wurtzite structure. It is revealed that the crystallite size decreases from 39 to 36 nm with the doping of Zr 3 wt%. The effect of Zr doping on surface morphology was observed and the elemental composition was confirmed by EDAX analysis. The optical transmission of ZnO films was influenced by Zr addition and the band gap measured from the absorption spectrum is increased from 3.24 to 3.26 eV. Pure and Zr dope Zno films are showing more than 90% transparancy in the visible region. Photoluminescence emissions indicated increase in concentration of oxygen vacancies with introduction of dopant. An inhouse setup was made to analyse the sensing performane of Pure and Zr doped ZnO thin films. The Zr doping gives more electrons in the ZnO matrix, which helps to improve the quantity of

adsorbed oxygen, leading to increased sensitivity and improve the NH$_3$ vapor sensor efficiency. The fabricated Zr doped Zno sensor showed good selectivity, fast response and recovery time to NH$_3$ vapour at room temperature.

Hense our present study indicated Zr (3 wt%) doped ZnO thin film exhibited the best properties with a good transmittance and it has wide band gap of 3.26 eV, whereas, photoluminescence emissions indicated increase in concentration of O$_2$ vacancies with introduction of dopant.

References

Al-Hardan N.H., Abdullah M.J. and Aziz A.A. (2009), The gas response enhancement from ZnO film for H$_2$ gas detection. *Applied Surface Science*, **255**, 7794–7797.

Anita, H., Nipin, K. and Singh R.C. (2016), Temperature dependent selective and sensitive terbium doped ZnO nanostructures. *Sensors and Actuators B*, **231**, 110–119.

Bahsi Z.B. and Oral A.Y. (2007), Effects of Mn and Cu doping on the microstructures and optical properties of sol–gel derived ZnO thin films. *Optical Materials*, **29,** 672–678.

Bharath S.P., Bangera K.V. and Shivakumar G.K. (2018), Enhanced gas sensing properties of indium doped ZnO thin films. *Superlattices and Microstructures*, **124**, 72–78.

Chao J., Chen Y., Xing S., Zhang D. and Shen W. (2019), Facile fabrication of ZnO/C nanoporous fibers and ZnO hollow spheres for high performance gas sensor. *Sensors and Actuators B*, **298**, 126927.

Corlu T., Karaduman I., Galioglu S., Akata B., Yıldırım M.A., Ates A. and Acar S. (2017), Low level no gas sensing properties of Cu doped Zno thin films prepared by Silar method. *Materials Letters*, **212**, 292–295.

Devi K.R., Selvan G., Hari Prasad, K. et al. (2020), Effect of Cu^{2+} doping on the structural, optical, and vapor-sensing properties of ZnO thin films prepared by SILAR method. *Journal of Materials Science: Materials in Electronics*, **31**, 16548–16560.

Dighavkar C. (2013), Characterization of nanosized zinc oxide based ammonia gas sensor. *Archives of Applied Science Research*, **5**(6), 96–102.

Gong Y., Wu X., Chen J., Li W., Han N., Zhang D. and Chen Y. (2019), Enhanced gas-sensing performance of metal@ZnO core–shell nanoparticles towards ppb–ppm level benzene: the role of metal–ZnO hetero-interfaces. *New Journal of Chemistry*, **43**, 2220–2230.

Hong M-H., Choi H., Kim Y., Kim T., Cho H.H., Driss Z., Driss D., Bouabidi A., Euchy S. and Park H-H. (2019), Ti doping effects on the Seebeck coefficient and electrical conductivity of mesoporous ZnO thin film. *Materials Chemistry and Physics*, **235,** 121757.

Hyojin K., Le Hung N., Eunseong A., Jung H. and Dojin K. (2010), Synthesis and Gas Sensing Properties of ZnO Nanostructures. *Journal of the Korean Physical Society*, **57**, 1784–1788.

Jayababu N., Poloju M. and Ramana Reddy M.V. (2018), Improved gas sensing performance of Al-doped ZnO/CuO nanocomposite, based ammonia gas sensor. *Materials Science and Engineering B*, **227,** 61–67.

Karmakar D., Dasgupta I., Das G.P. and Kawazoe Y. (2007), High temperature ferromagnetism in Fe-doped ZnO: a density functional investigation. *Materials Transactions*, **48**, 2119–2122.

Krishnan V.G. (2017), Influence of Ba doping concentration on the physical properties and gas sensing performance of ZnO nanocrystalline films: automated nebulizer spray pyrolysis (ANSP) method. *Optik*, **141**, 83–89.

Kwak D., Lei Y. and Maric R. (2019), Ammonia gas sensors: a comprehensive review. *Talanta*, **204**, 713–730,

Lee J.H.and Park B.O. (2003), Transparent conducting ZnO:Al, In and Sn thin films deposited by the sol–gel method. *Thin Solid Films*, **426**(1–2), 94–99.

Lee J.H., Lin P., Ho J.C. and Lee C.C. (2006), Chemical solution deposition of $Zn_{1-x}Zr_xO$ thin films as active channel layers of thin-film transistors. *Electrochemical and Solid State Letters*, **9**(4), G117.

Lukas S.M. and Judith M.D. (2007), ZnO – nanostructures, defects, and devices. *Materials Today*, **10**(5), 40–48.

Mani G.K. and Rayappan J.B. (2014), Selective detection of ammonia using spray pyrolysis deposited pureand nickel doped ZnO thin films. *Applied Surface Science* **311**, 405–412.

Mani G.K. and Rayappan J.B.B. (2015), A highly selective and wide range ammonia sensor—nanostructured ZnO:Co thin film. *Materials Science and Engineering B,* **191**, 41–50.

Naushad M. (2014), Surfactant assisted nano-composite cation exchanger: Development, characterization and applications for the removal of toxic Pb^{2+} from aqueous medium. *Chemical Engineering Journal*, **235**, , 100–108.

Naushad M. and ALOthman Z.A. (2015), Separation of toxic Pb2+ metal from aqueous solution using strongly acidic cation-exchange resin: analytical applications for the removal of metal ions from pharmaceutical formulation. *Desalination and Water Treatment*, **53** , 2158–2166.

Naushad M., ALOthman Z.A., Awual M.R., Alam M.M. and Eldesoky G.E. (2015), Adsorption kinetics, isotherms, and thermodynamic studies for the adsorption of Pb2+ and Hg2+ metal ions from aqueous medium using Ti(IV) iodovanadate cation exchanger. *Ionics (Kiel)*, **21**, 2237–2245.

Naushad M., Mittal A., Rathore M. and Gupta V. (2015), Ion-exchange kinetic studies for Cd(II), Co(II), Cu(II), and Pb(II) metal ions over a composite cation exchanger. *Desalination and Water Treatment*, **54**, 2883–2890.

Naushad M., Sharma G. and Alothman Z.A. (2019), Photodegradation of toxic dye using Gum Arabic-crosslinked-poly(acrylamide)/Ni(OH)2/FeOOH nanocomposites hydrogel. *Journal of Cleaner Production*, **241**, 118263.

Nkosi S.S., Kortidis I., Motaung D.E. and Kroon R.E., Leshabane N., James T. and Ndwandwe O.M. (2020), The effect of stabilized ZnO nanostructures green luminescence towards LPG sensing capabilities. *Materials Chemistry and Physics*, **242**, 122452.

Norris B.J., Anderson J., Wager J.F. and Keszler D.A. (2003), Spin-coated zinc oxide transparent transistors. *Journal of Physics D: Applied Physics*, **36**, L105–L107.

Pandey S. (2016), Highly sensitive and selective chemiresistor gas/vapor sensors based on polyaniline nanocomposite: A comprehensive review. *Journal of Science: Advanced Materials and Devices*, **1**(4), 431-453.

Pandey S. and Nanda K.K. (2015), Au nanocomposite based chemiresistive ammonia sensor for health monitoring. *In ACS Sensors*, **1**(1), 55–62.

Pandey S. and Ramontija J. (2016), Rapid, Facile microwave-assisted synthesis of xanthan gum grafted polyaniline for chemical sensor, *International Journal of Biological Macromolecule*, **89**, 89-98.

Paraguay F., Miki-Yoshida M., Morales J., Solis J. and Estrada W. (2000), Influence of Al, In, Cu, Fe, and Sn dopants on the response of thin film ZnO gas sensor to ethanol. *Thin Solid Films*, **373**, 137–140.

Patil V.L., Vanalakar S.A., Tarwal N.L., Patil A.P., Dongale T.D., Kim J.H. and Patil P.S. (2019), Construction of Cu doped ZnO nanorods by chemical method for Low temperature detection of NO_2 gas. *Sensors and Actuators,* **299**, 111611.

Qadri S.B., Kim H., Horwitz J.S. and Chrisey D.B. (2000), Transparent conducting films of $ZnO–ZrO_2$: Structure and properties. *Journal of Applied Physics*, **88**, 6564–6566.

Radhi Devi K., Selvan G., Karunakaran M., Loyola Poul Raj I., Ganesh V. and AlFaify S. (2020), Enhanced room temperature ammonia gas sensing properties of strontium doped ZnO thin films by cost-effective SILAR method. *Materials Science in Semiconductor Processing*, **119**, 105117.

Renitta A. and Vijayalakshmi K. (2017), High performance hydrogen sensor based on Mn implanted ZnO nanowires array fabricated on ITO substrate. *Materials Science and Engineering: C*, **77**, 245–256.

Sankar Ganesh R., Durgadevi E., Navaneethan M., Patil V.L., Ponnusamy S., Muthamizhchelvan C., Kawasaki S., Patil P.S. and Hayakawa Y. (2017), Tuning the selectivity of NH_3 gas sensing response using Cu-doped ZnO nanostructures. *Sensors and Actuators,* **269**, 331–341.

Sankar Ganesh R., Mani G.K., Elayaraja R., Durgadevi E., Navaneethan M., Ponnusamy S., Tsuchiya K., Muthamizhchelvan C. and Hayakawa Y. (2018), ZnO hierarchical 3D-flower like architectures and their gas sensing properties at room temperature. *Applied Surface Science*, **449**, 314–321.

Shingange K., Tshabalala Z.P., Ntwaeaborwa O.M., Motaung D.E. and Mhlongo G.H. (2016), Highly selective NH_3 gas sensor based on Au loaded ZnO nanostructures prepared using microwave-assisted method. *Journal of Colloid and Interface science,* **479**, 127–138.

Singh S.K., Dutta D., Das S., Dhar A. and Paul M.C. (2020), Synthetic and structural investigation of ZnO nano-rods, hydrothermally grown over Au coated optical fiber for evanescent field based detection of aqueous ammonia. *Materials Science in Semiconductor Processing*, **107**, 104819.

Tauc J., Grigorovici R. and Vancu A. (1966), Optical properties and electronic structure of amorphous germanium. *Physica Status Solidi (b)*, **15**(2), 627–637.

Vijayprasath G., Murugan R., Ravi G., Mahalingam T. and Hayakawa Y. (313), Characterization of dilute magnetic semiconducting transition metal doped ZnO thin films by sol-gel spin coating method. *Applied Surface Science*, **313**, 870.

Wang C., Yin L., Zhang L., Xiang D. and Gao R. (2010), Metal oxide gas sensors: sensitivity and influencing factors. *Sensors*, **10**(3), 2088–2106.

Wang M., Wang J., Chen W., Cui Y. and Wang L. (2006), Effect of preheating and annealing temperatures on quality characteristics of ZnO thin film prepared by sol–gel method. *Materials Chemistry and Physics*, **97**, 219–225.

Zhao M., Wang X., Ning L., Jia J., Li X. and Cao L. (2011), Electrospun Cu-doped ZnO nanofibers for H_2S sensing. *Sensors and Actuators B*, **156**, 588–592.